Electrical recordings from rat cardiac muscle cells using field-effect transistors

Christoph Sprössler,[1,2] Morgan Denyer,[2] Steve Britland,[3] Wolfgang Knoll,[1,2] and Andreas Offenhäusser[1,*]
[1]*Max-Planck-Institute for Polymer Research, Ackermannweg 10, D-55128 Mainz, Germany*
[2]*Frontier Research Program, The Institute of Physical and Chemical Research (RIKEN), 2-1 Hirosawa, Wako-shi, Saitama 351-0198, Japan*
[3]*School of Pharmacy, University of Bradford, West Yorkshire BD7 1DP, England*
(Received 27 January 1998; revised manuscript received 12 April 1999)

Extracellular electrophysiological recordings were made from cardiac cells cultured for up to seven days over microfabricated arrays of field-effect transistors. The recorded signals can be separated mainly into two types of cell transistor couplings: one that can be explained entirely by purely passive circuitry elements, and a second where voltage-gated ion channels contribute greatly to the measured extracellular signal. [S1063-651X(99)12008-7]

PACS number(s): 87.17.Nn, 87.80.Tq, 73.40.Mr

I. INTRODUCTION

Impulse propagation in the cardiac muscle tissue is determined by both active (including ion channels, ion exchangers, and ion pumps) and passive (membrane resistance and capacitance, size and shape of individual cells, cell assemblage, topology and density of gap junctions, and the spatial organization of the extracellular space) properties of the cardiac muscle cells. The spontaneous rhythmic electrical and mechanical activity of cultured myocardiac cells is widely used to study cardiac physiology. Electrical activity in tissue culture is usually recorded using intracellular glass micropipettes and patch clamp pipettes, or metal electrodes. However, it is difficult to use these techniques for extended periods of time because of cell movement, breakage, or damage. By using semiconductor planar technology, substrate-embedded metal microelectrodes (MME's) of various sizes and shapes have been built for long term recording from cardiac cells [1–3] and neurons [4–6]. Field-effect transistors (FETs) have also been used to record from electrically active cells and tissues. A large FET with a nonmetallized gate was applied to record extracellular voltage from muscle tissue [7], and FET arrays with ''floating'' gold gates have been used to record from hippocampal slices [8]. More recently, recordings from individual invertebrate neurons were made using FETs with open gates [9].

Various methods of describing the coupling of signals from electrogenic cells with either MME or FET have been proposed in the literature. The coupling of signals from large invertebrate neurons with MME was described using equivalent circuit models in a qualitative [11] way or by calculating the extracellular potential field generated by a transmembrane current using the finite element method [12]. The coupling of signals from large invertebrate neurons with FET was described in detail using equivalent circuit models and distributed systems as given by two-dimensional cable theory [9,10]. Recently, these models have been modified taking into account the contribution of voltage-gated ion channels of the cell membrane in the contact region [13].

We report here the development and application of a FET based recording device from which extracellular recordings from a monolayer of cultured myocardial cells can be made simultaneously with intracellular measurements of the membrane voltage. We present five representative measurements of the various types of couplings. We simulate the size and shape of the recorded extracellular signals by means of a model based on passive circuit elements in combination with time- and voltage-dependent properties of membrane currents modeled using equations of the form originally proposed by Hodgkin and Huxley. This clearly indicates the influence of voltage-gated ion channels on the recorded extracellular signals.

II. EXPERIMENTAL SETUP

Field-effect transistor arrays used in this study were fabricated using standard silicon planar technology. The array consisted of 16 *p*-channel FETs with nonmetallized gates [14]. The sizes of the gates ranged between 28×9 μm^2 down to 10×1 μm^2 and were arranged in a 4×4 matrix with the centers 200 μm apart. The chips were mounted on standard 28 DIL ceramic chip carriers (NGK Spark Plug Co., LTD, Japan), wire-bonded, and encapsulated using a silicone polymer (Sylgard 184 and 96-083, Dow Corning). Together with a glass ring affixed to the chip carrier, the encapsulated device forms a small culture dish. Electrical measurements with the FET were carried out with a Ag/AgCl wire as a reference electrode which defines the gate potential. Measurements were performed in the third quadrant in which the usual driving conditions for the drain-source voltage (V_{DS}) was -2.0 V and the Ag/AgCl-source voltage (V_{GS}) was -2.0 V, resulting in a transconductance ($g_m = dI_{DS}/dV_{GS}$) between 0.1 and 0.4 mS depending on the gate size. In these conditions the leakage current from the source (I_{GS}) was negligible.

The cardiac myocytes were prepared following a technique that has been described in detail elsewhere [15]. Briefly, the hearts were removed from one to three-day old rats, finely minced and dissociated and plated onto the recording devices in a serum-containing medium. Prior to plating, the FET arrays were cleaned with 25% sulfuric acid, washed with Milli-Q water, sterilized with 70% ethanol, and coated with fibronectin [16]. The fibronectin (10 μg/ml in

*Electronic address: offenhaeusser@mpip-mainz.mpg.de

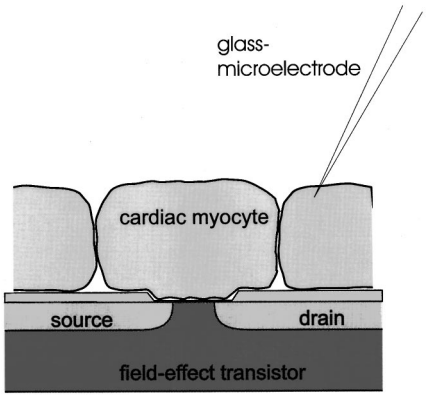

FIG. 1. Schematic view of the cell-device assembly. A monolayer of rat cardiac myocytes is cultured on the FET surface for both an extracellular recording by FET and intracellular recording by microelectrode. The dimensions of the assembly are as follows: cardiac myocyte, ca. 70 μm$\times$25 μm; FET, gate length 1–12 μm and gate width 8–28 μm.

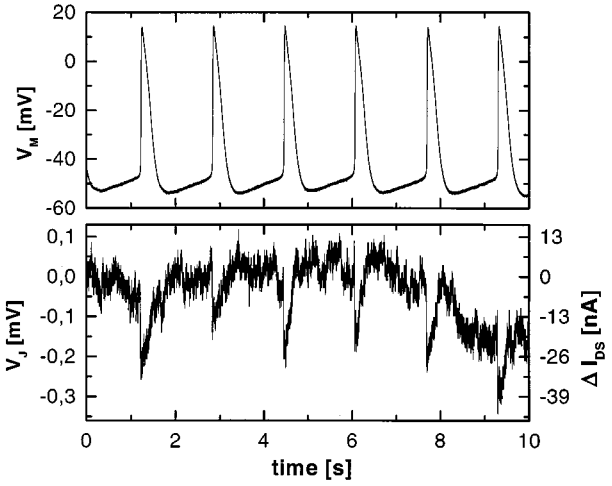

FIG. 2. Electrical recording from rat cardiac myocytes after four days in culture. Measurements performed simultaneously by FET (lower trace) and microelectrode (upper trace) for 10 sec. The extracellularly recorded trace is scaled as drain-source current I_{DS} and as effective voltage in the junction area V_J determined by the transfer characteristics.

HBSS) was applied to the devices for a period of 1 hr, after which the substrates were washed with sterile Milli-Q water and allowed to air dry in sterile conditions. Finally, approximately 80 μl of a suspension containing between 5×10^5 and 9×10^5 cells/ml were used to fill the culture dish of the FET array, which resulted in a cell density of approximately 3×10^7 cells/cm^2. The culture was incubated at 37°C in a humidified atmosphere. Under these conditions, within 2–3 days, a confluent monolayer of cells exhibiting spontaneous rhythmic activity developed.

The electrical activity of these cells was studied starting on the third day after plating. For recording, the FET array was connected to a specially built 16-channel preamplifier mounted under the microscope [17]. During experiments, the offset currents arising from the driving conditions of all 16 channels were compensated and recorded signals were amplified by a gain of 100. No filtering other than a 3 kHz low-pass filter unit (3 dB) was used which was included in the amplification system. Up to four selected channels were monitored using a computer with an ADC card connected to the electronic setup. In some experiments, simultaneous extracellular and intracellular recordings were made using glass microelectrodes filled with 3 M KCl and mounted in a holder-preamplifier headstage (Luigs & Neumann, Germany). In the case of intracellular recordings, the headstage signal was amplified using a whole cell amplifier (List Electronic, Germany) that could be connected to the computer and to an oscilloscope. The temperature was kept constant at 37 °C using a heater pad fitted to the FET preamplifier. In Fig. 1 the principal setup for the described experiment is schematically shown.

III. RESULTS AND DISCUSSIONS

In fully developed cultured cardiac cells, the action potential is generated by the sodium, calcium, and potassium currents across the cell membrane. The inward sodium current is the initial event triggering a fast-rising action potential. The calcium current carries the plateau phase of the action potential and the outward potassium current repolarizes the cell.

Figure 2 shows typical recordings from cardiac muscle cells performed simultaneously with an intracellular microelectrode (upper trace) and a FET (lower trace). Intracellular recordings were made from cells grown several μm away from the recording site of the FET. The fast rising of the intracellular voltage V_M (microelectrode, upper trace of Fig. 2) causes first a sharp increase followed by a long-lasting decrease in the drain-source current I_{DS} of the transistor (FET, lower trace of Fig. 2). [Due to the measurement conditions (third quadrant, negative driving voltages and therefore negative drain-source current), a positive voltage change at the gate causes an increase in I_{DS} (decrease of absolute I_{DS}).] From the transfer characteristics of each transistor, the corresponding gate-source voltage V_{GS} can be calculated, which corresponds to the voltage in the junction area V_J, and it was found that extracellular action potentials with amplitudes larger than 0.3 mV could be recorded. The recorded voltages were about 5–10 times greater than the background noise.

In Figs. 3 and 4, a more detailed view of typical recordings is shown. Figure 3 I shows the action potential (AP) of cardiac myocytes recorded with a glass microelectrode. The overall duration of the AP was between 300 and 400 ms.

In less than 5% of the experiments, extracellular signals with sharp peaks in the rising phase of the AP were recorded (Fig. 3 II). The duration of these positive peaks was between 1 and 2 ms with amplitudes between 0.2 and 1.0 mV. In analogy to the nomenclature used for the description of neuron-transistor coupling [9,10] we will use the term ''*A*-type'' to describe this kind of signal.

Figure 3 III shows the largest extracelluar signal we recorded with the FETs. The signal is monophasic and has a shape almost identical to the intracellular signals we observed (Fig. 3 I). The amplitudes of these signals, which lasted approximately 300 ms, was up to 25 mV. Signals of this type were observed in less than 5% of the experiments

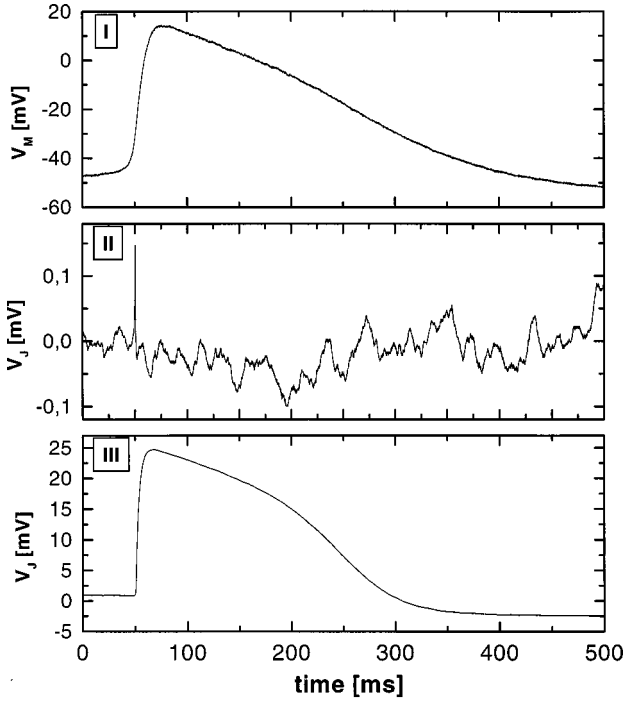

FIG. 3. More detailed view of the action potential from Fig. 2 recorded with glass microelectrode (trace I). The other traces show extracellular recordings with a sharp peak in the rising phase of the AP (''*A*-type,'' trace II) and with a shape almost identical to the intracellular signal (''*B*-type,'' trace III).

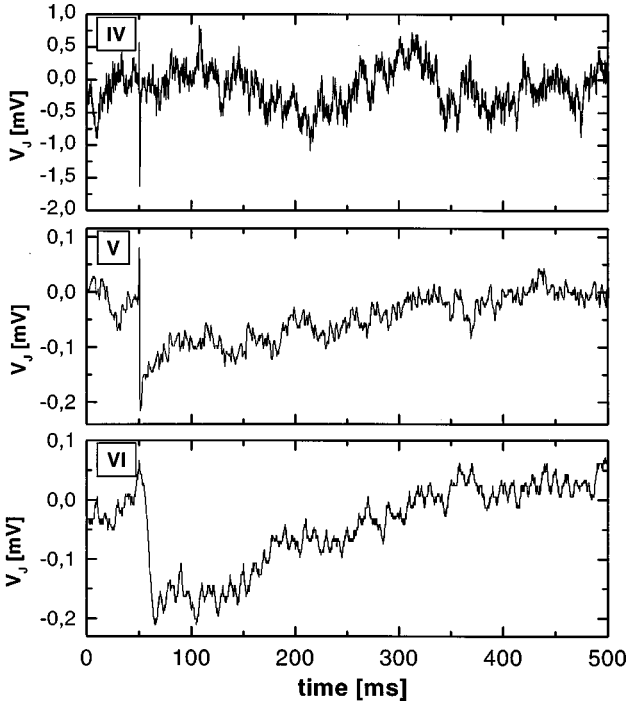

FIG. 4. Extracellular recording observed most often with a sharp positive followed by a negative peak (''*D*1-type,'' trace IV). In the other traces the sharp peaks at the beginning of the AP are followed by a second part lasting much longer (''*D*2-type,'' trace V; ''*D*3-type,'' trace VI).

and will be called ''*B*-type'' to describe it analogously to [9,10].

Figure 4 IV shows the type of signal we observed most often ($>75\%$). The sharp rise of the extracellular signals at the beginning of the AP represents about 10–50% of the overall signal. The second part of the signal with a negative peak seems to resemble the overshooting Na^+ component of the action potential. The overall duration of this type of extracellular signal was about 5–10 ms with amplitudes up to 8 mV. We will use the term ''*D*1-type'' to describe this signal.

Figure 4 V shows another type of extracellular recording. Again, the sharp rise of the extracellular signals at the beginning of the AP represents about 10–50% of the overall signal. The second part of the signal starts with a negative peak similar to the one described in Figure 4 IV. After a short recovery, a second part followed and lasted much longer. The negative parts of these signals seems to resemble a combination of the overshooting Na^+ spike and Ca^{2+} component of the action potential. The overall duration of the second part of this type of extracellular signal was about 200–300 ms with amplitudes up to several hundred μV. We will use the term ''*D*2-type'' to describe this signal, which we observed in less than 5% of our recordings.

Figure 4 VI shows extracellular signals that we recorded in approximately 10% of our experiments. Again, the sharp rise in the extracellular signals at the beginning of the AP represents about 10–50 % of the overall signal. The second part of the signal shows only a single negative peak similar to the last part described in Fig. 4 V and it is probable that this negative part is dominated by the Ca^{2+} component of the action potential. The overall duration of the second part of this type of extracellular signal was about 200–300 ms with amplitudes up to several hundred μV. We will use the term ''*D*3-typ'' to describe this signal.

In order to explain the recorded signals, the point-contact model shown in Fig. 5 was used. The junction is described by the passive elements of gate capacitance C_{JG}, membrane capacitance C_{JM}, and seal resistance R_J in addition to the Na^+, Ca^{2+}, K^+ and leakage currents modeled by Hodgkin-Huxley elements. The extracellular voltage $V_J(t)$ was simu-

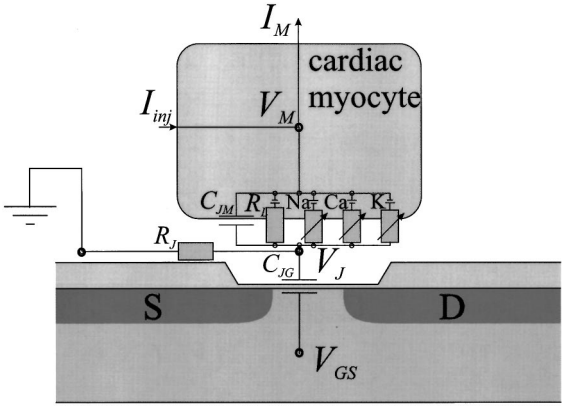

FIG. 5. Equivalent circuitry used for description of the dependence of voltage V_J in the junction area coupled into the FET device on the membrane voltage V_M. In addition to the passive electronic elements (C_{JG},C_{JM},R_J) in the junction area, the ionic currents of Na^+, Ca^{2+}, K^+ and the leakage current modeled by Hodgkin and Huxley are considered. I_{inj} represents the current injected by the neighboring cells, whereas I_M represents the sum of the ionic currents through the membrane used for the simulation.

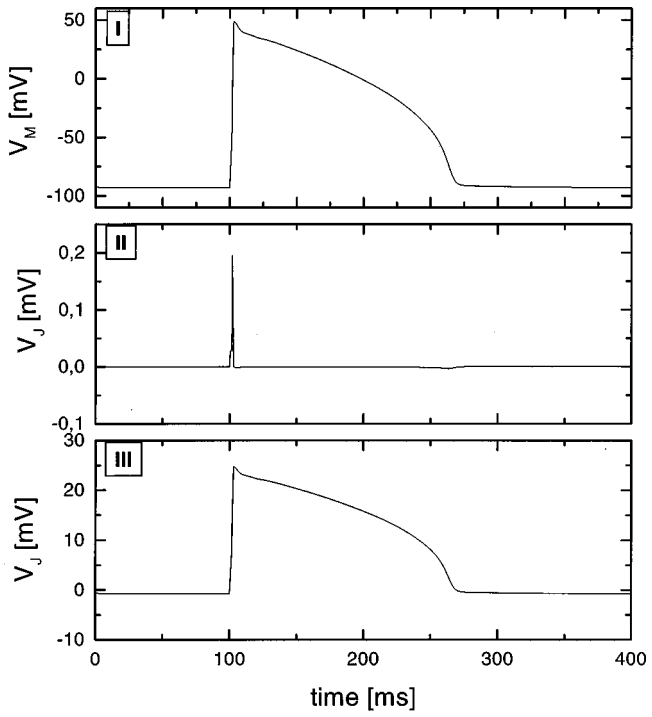

FIG. 6. Using the HEART software based on the theory of Hodgkin and Huxley for a standard single-ventricular cell, the action potential was simulated (trace I). The ''*A*-'' and ''*B*-types'' can be explained only by passive electronic elements. The simulation of the ''*A*-type'' (trace II) uses mainly C_{JM} and R_J acting as high-pass elements. The ''*B*-type'' is mainly determined by the ratio R_L^{JM}/R_J (trace III).

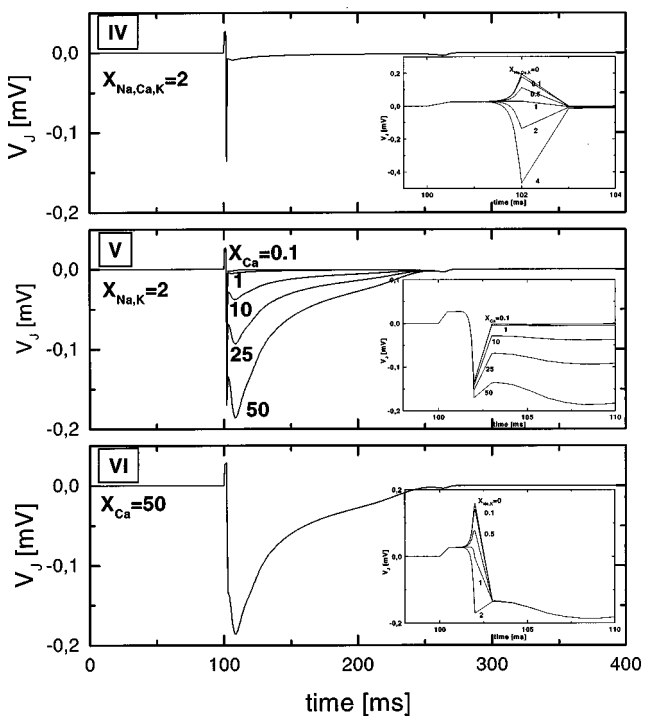

FIG. 7. In addition to the passive electronic elements, ionic currents were considered. The short negative peak in trace IV (''*D*1-type'') is given by an enhancement of the ionic current in the junction area (variations of $X_{Na,Ca,K}$ are shown in the inset in a detailed view). Signals of ''*D*2'' (trace V) and ''*D*3'' (trace VI) type can be explained by an enhancement of the Ca^{2+} current in the junction area (factor $X_{Ca} \gg 1$). The sharp negative peak (trace V) in the rising phase of the AP is only visible if the Na^+ current is also enhanced (factor $X_{Na} > 1$).

lated according to Eq. (1) considering the current $I_{JM}^M = C_{JM}[d(V_M - V_J)/dt] + \Sigma_i I_{JM}^i$ through the membrane in contact with the gate together with the current $I_J = (1/R_J)V_J$ along the cleft between membrane and gate and the current $I_{JG} = C_{JG}(dV_J/dt)$ through the gate oxide.

$$C_{JG}\frac{dV_J}{dt} + \frac{1}{R_J}V_J = C_{JM}\frac{d(V_M - V_J)}{dt} + \sum_i I_{JM}^i . \qquad (1)$$

The current through the ion channels I_{JM}^i can be simulated by voltage-gated time-dependent and -independent conductivities G^i based on the theory of Huxley and Hodgkin [18]. We calculated both the intracellular voltage V_M and the various currents through the membrane I_{JM}^i using the OXSOFT HEART simulation software in which models of single cardiac cells have been implemented by the Noble group [19]. To simulate the action potential shown in Fig. 3 I, we used the standard single-ventricular cell model [20]. In this model the cardiac cell with a length of 120 μm and a diameter of 15 μm is assumed, resulting in an overall membrane capacitance of 200 pF ($c_M = 1.5$ μF/cm^2). The following maximal ionic conductances were used: $g_{Na}^0 = 18.75$ mS/cm^2, $g_K^0 = 7.5$ mS/cm^2, and $g_{Ca}^0 = 8$ mS/cm^2. The action potential is elucidated by a stimulus current I_{inj} of 6 nA lasting for 2 ms and starting at 100 ms. Using these parameters, the duration of the simulated AP (Fig. 6 I) is about 170 ms with an amplitude of about 140 mV. Shape and overall length differs from the measured APs which might be due to the interaction with neighboring cells (compound AP), temperature, or quantitative differences in channel conductivities which we did not adapt.

For the simulation of the extracellular voltage $V_J(t)$ we numerically integrated Eq. (1). For the calculation we considered the influence of time-dependent current I_{Na}, I_{Ca}, I_K, and leakage current. The contribution of other currents was neglected. For the passive elements in the contact area a gate capacitance of $C_{JG} = 0.4$ pF and a seal resistance $R_J = 1$ MΩ were chosen. A membrane capacitance of $C_{JM} = 1.5$ pF was used assuming a contact area of about 100 μm^2. The simulated signals are shown in Figs. 6 and 7.

The ''*A*-type'' extracellular signal (Fig. 6 II) can be explained by a convolution of the intracellular voltage $V_M(t)$ with high-pass filter elements mainly consisting of the capacitance of the membrane C_{JM} and the seal resistance R_J of the junction, neglecting contributions from ion channels and gate capacitance. Therefore, shape and amplitude of this peak can be described by the time constant ($\tau_H = C_{JM}R_J$) of this high-pass filter element.

For the ''*B*-type'' junction (Fig. 6 III), capacitive current is negligible and current flow is determined mainly through the ratio R_L^{JM}/R_J. This kind of signal can be explained by assuming that the seal resistance R_J of the junction is in the range of the leakage membrane resistance R_L^{JM} in the junction with a reversal voltage equal to the membrane voltage.

This can be explained either by assuming that the seal resistance R_J is a factor of 1000 larger than expected or by the fact that the leakage membrane resistance R_L^{IM} is small compared to the usual membrane resistance (leaky membrane model [10]).

In order to simulate the ''*D*1-type'' extracellular signal, we scaled the sodium, potassium, and calcium current densities in the contact area by factors of $X_{Na,Ca,K}=0,0.1,0.5,1,2,4$ as shown in Fig. 7 IV (inset). We observed a compensation of the capacitive signal and a negative response when the ion channel current density in the contact area is enhanced ($X_{Na,Ca,K}>1$) compared to the overall membrane similar to the *C*1 junction introduced for the neuron-silicon coupling [13]. An almost complete vanishing signal is observed in the case of even by distributed current densities ($X_{Na,Ca,K}=1$) except for the capacitive transient of the ''stimulus current'' I_{inj}, and a signal similar to the ''*A*-type'' junction is found in the case of reduced current densities ($X_{Na,Ca,K}<1$). This model allows one to explain the second part of the signal as being due to enhanced ion current densities. The upstroke at the beginning of the signal seems to be due to the stimulus current I_{inj} that comes from neighboring cells. The best simulation of the measured signal (Fig. 4 IV) was obtained with $X_{Na,Ca,K}=2$.

The ''*D*2-type'' extracellular signal was simulated by scaling the calcium current density in the contact area by factors of $X_{Ca}=0.1,1,10,25,50$ while keeping the other ion current densities in the contact area twice the current densities in the overall membrane ($X_{Na,K}=2$). Figure 7 V shows again the positive peak due to stimulus current and the negative peak mainly due to the enhanced sodium current density followed by a second part when the calcium current density was greatly enhanced. The inset of Fig. 7 V shows that this change in calcium current density will not influence the negative peak due to sodium current. The best simulation of the measured signal (Fig. 4 V) can be obtained with $X_{Ca}=30$.

In order to simulate the ''*D*3-type'' extracellular signal, the calcium current density in the contact area was kept constant at $X_{Ca}=50$ while sodium and potassium current densities in the contact area were scaled by factors of $X_{Na,K}=0,0.1,0.5,1,2$. Figure 7 VI shows again the positive peak due to stimulus current and a long lasting negative peak mainly due to the enhanced calcium current density. The inset of Fig. 7 VI shows that reduced or regular sodium and potassium current densities have little influence on the shape of the negative peak. The best simulations of the measured signal (Fig. 4 VI) were obtained with $X_{Ca}=50$ and $X_{Na,K}=1$.

IV. CONCLUSION

To get a better understanding of the coupling, we have to discuss various possible situations. In a first attempt we are assuming that there is no effect due to the confluent cell layer, i.e., the coupling of the cardiac myocyte is discussed as a single cell coupling. From the simulations of the signals we have measured so far, in addition to experimental data for the specific membrane resistance and capacitance ($c_M=1\cdots2$ μF/cm^2, $r_M=10\cdots20$ kΩ cm^2) for cardiac muscle cells and assuming a circular coupling geometry with a radius of about 5 μm we can estimate the seal resistance of the coupling [10]. With these assumptions, the seal resistance of the cell to the substrate-embedded detector ($R_J\approx1$ MΩ) is in the range of the strong-coupling measurements done with invertebrate neurons ($R_J>2$ MΩ) [10]. In this model the specific seal resistance $r_J=\rho/d_J=5\pi R_J$ depends on the specific resistance of the electrolyte ρ and the cell membrane-substrate distance d_J: using a specific resistance of $\rho=100\,\Omega$ cm, this results in distances d_J in the range of 50 nm. Studies of cell-substrate separation using reflection interference contrast microscopy showed that cardiac muscle cells have only a few focal contacts in this range [21]. Although these data were obtained with glass cover slips, we think they are most likely relevant to the problem of cell adhesion on silicon oxide due to the similar surface chemistry of glass and silicon oxide, both modified with fibronectin. These studies indicate that the high seal resistance might be influenced by the confluent cell monolayer.

From our simulations, it is obvious that the signal is determined not only by the linear circuit consisting of passive membrane elements. Current injection from the cell into the contact area plays a major role. Interestingly, we found from our simulations that the positive part of the ''*D*-type'' signals is mainly due to the ''stimulus current'' that comes from neighboring cells and will remain the only signal if an equal current density for the contact area and the overall cell membrane is assumed. From our simulations we found that the negative part of the ''*D*-type'' signals is due to an enhanced current density in the contact area. The shape and duration of this part seems to be determined by sodium and/or calcium currents. Surprisingly, we never found any signal that was dominated by the potassium current.

The influence of the ion currents on the recorded signals opens up the possibility of using this recording device for current measurements that might be of interest for long-term investigations of membrane current profiles and pharmaceutical tests. The model circuit considering the ionic current through the membrane, in addition to the passive membrane elements, shows good agreement with the experimental results. In addition, we have tested the cardiac muscle cell/FET assemblies over several days, recording similar signals from the corresponding transistors, indicating the possibility of maintaining long-term electrical contact with the cultured cells.

ACKNOWLEDGMENTS

Professor A. S. G. Curtis and Dr. M. Riehle (University of Glasgow) are acknowledged for introducing the method of cardiac cell culture. We would like to thank Mr. Lacher and Dr. Zetterer (both from the Institut für Mikrotechnik, Mainz) for support in preparing the FETs. Dr. A. Maelicke (University of Mainz) and his co-workers are acknowledged for their support with animal facilities. This work was partially funded by the Deutsche Forschungsgesellschaft (Grant No. Of 22/2-1), the Ministerium für Bildung, Wissenschaft, Forschung und Technologie (BMBF) (Proj.-No. 0310852), and the British-German Academic Research Collaboration (DAAD/BC).

[1] C.A. Thomas, P.A. Springer, G.E. Loeb, and Y. Berwald-Netter, L.M. Okun, Exp. Cell Res. **74**, 61 (1972).
[2] D.A. Israel, W.H. Barry, D.J. Edell, and R.G. Mark, Am. J. Physiol. **247**, H669 (1984).
[3] P. Connolly, P. Clark, A.S.G. Curtis, J.A.T. Dow, and C.D.W. Wilkinson, Biosens. Bioelectron. **5**, 223 (1990).
[4] G.W. Gross, E. Rieske, G.W. Kreutzberg, and A. Meyer, Neurosci. Lett. **6**, 101 (1977).
[5] J.L. Novak and B.C. Wheeler, IEEE Trans. Biomed. Eng. **33**, 196 (1986).
[6] R.J.A. Wilson *et al.*, J. Neurosci. Methods **53**, 101 (1994).
[7] P. Bergveld, J. Wiersma, and H. Meertens, IEEE Trans. Biomed. Eng. **23**, 136 (1972).
[8] D.T. Jobling, J.G. Smith, and H.V. Wheal, Med. Biol. Eng. Comput. **19**, 553 (1981).
[9] P. Fromherz, A. Offenhäusser, T. Vetter, and J. Weis, Science **252**, 1290 (1991).
[10] P. Fromherz, C.O. Müller, and R. Weis, Phys. Rev. Lett. **71**, 4079 (1996); R. Weis and P. Fromherz, Phys. Rev. E **55**, 877 (1997).
[11] W.D. Regehr, J. Pine, C.S. Cohan, M.D. Mischke, and D.W. Tank, J. Neurosci. Methods **30**, 91 (1989).
[12] R. Lind, P. Connolly, C.D.W. Wilkinson, and R.D. Thompson, Sens. Actuators B **3**, 23 (1991).
[13] R. Schätzhauer and P. Fromherz, Eur. J. Neurosci. **10**, 1956 (1998).
[14] A. Offenhäusser, C. Sprössler, M. Matsuzawa, and W. Knoll, Biosens. Bioelectron. **12**, 819 (1997).
[15] S. Bhatti, G. Zimmer, and J. Bereiter-Hahn, J. Mol. Cell. Cardiol. **10**, 995 (1989).
[16] H.M. Piper, R. Spahr, I. Probst, and P.G. Spieckermann, Basic Res. Cardiol. **80**, 175 (1985); E. Lundgren, L. Terracio, and T.K. Borg, Basic Res. Cardiol. **80**, 69 (1985).
[17] C. Sprössler, D. Richter, M. Denyer, and A. Offenhäusser, Biosens. Bioelectron. **13**, 613 (1998).
[18] A.F. Huxley and A.L. Hodgkin, J. Physiol. (London) **116**, 449 (1952).
[19] D. DiFrancesco and D. Noble, Philos. Trans. R. Soc. London, Ser. B **B307**, 353 (1985).
[20] Y. E. Earm and D. Noble, Proc. R. Soc. **240**, 83 (1990); D. Noble, OXSOFT HEART Manual, version 4.8 (Oxsoft Ltd., Oxford, 1997).
[21] W. J. Parak *et al.* (unpublished).